Analysis of Ring-Stiffened Shells of Revolution under Combined Thermal and Mechanical Loading

DAVID BUSHNELL*
Lockheed Palo Alto Research Laboratory, Palo Alto, Calif.

An energy formulation is used in conjunction with the method of finite differences for calculation of stresses, buckling loads, and vibration frequencies of complex shells of revolution. The development is similar to that used in the finite element method and is ideally suited for programing on the digital computer. Numerical results for stress and stability are obtained for ring-stiffened cylinders and conical shells with combined mechanical and thermal loads.

Nomenclature

A = discrete ring cross-sectional area
C_{ij},[C] = constitutive equation coefficients [Eq. (6)]
d_1,d_2 = radial, axial components of reference surface discontinuity (Fig. 3)
E = Young's modulus
E_{11},E_{12},E_{22} = $E_1/(1-\nu_{12}\nu_{21})$, $\nu_{21}E_{11}$, $E_2/(1-\nu_{12}\nu_{21})$
e_1,e_2 = radial, axial components of discrete ring eccentricity (Fig. 2)
G = shear modulus
H = radial line load applied at discrete ring centroid (Fig. 2)
h = finite-difference mesh spacing
I = discrete ring moment of inertia (subscripted)
J = discrete ring torsion constant
$KA1,KA2,\ldots$ = boundary condition designators for A end of shell meridian
$KB1,KB2,\ldots$ = boundary condition designators for B end of shell meridian
m = shell mass/area
M = line moment applied at discrete ring centroid (Fig. 2), bending moment resultants (subscripted)(Fig. 1)
n = number of circumferential waves
N = in-plane stress resultants (subscripted)(Fig. 1)
p_1,p_2,p_3 = pressure components (Fig. 1)
q_i = dependent variables of energy
r = parallel circle radius (Fig. 1)
R = radius of curvature (subscripted)(Fig. 4)
s,S = arc length measured from point A
S = shear force/length applied to discrete ring axis (Fig. 2)
[S] = stress vector [Eqs. (7) and (8)]
t = shell thickness
T = temperature rise above zero-stress state
T_s,T_r = kinetic energy of shell, ring
u,u^* = meridional, axial displacement (Figs. 1 and 2)
U_s,U_r = strain energy of shell, ring
U_{p1},U_{p2} = potential energy of line loads, distributed load
U_c = constraint "energy"
v,v^* = circumferential displacement (Fig. 1)
V = axial line load applied to ring centroid (Fig. 2)
w,w^* = normal, radial displacement (Figs. 1 and 2)
x,y = axis system attached to discrete ring centroid (Fig. 2)
z = distance from reference surface, positive outward (Fig. 1)
α = coefficient of thermal expansion
γ = rotation around normal [Eq. (11), Fig. 1]
ϵ = reference surface strains (subscripted) [Eq. (10)]
[ϵ] = strain vector [Eqs. (7) and (10)]
ε = strain, a function of z [Eq. (3)]
λ_i = Lagrange multipliers for constraint conditions
λ = eigenvalue
$\varkappa$ = reference surface changes in curvature [Eq. (10)]
Ω = eigenfrequency
ψ = rotation about meridian [Eq. (11), Fig. 1]
χ = rotation of meridian [Eq. (11), Fig. 1]
ρ = discrete ring material density
σ = normal stress
τ = shear stress
θ = circumferential coordinate
ν = Poisson's ratio

Subscripts

c = ring centroid
i = ith mesh point
min,max = minimum, maximum
n = circumferential wave number, also with respect to axis normal to shell meridian
$_0$ = prebuckling quantity
p = polar
r = ring quantity
s = shell, or with respect to axis parallel to shell meridian
$,t$ = differentiation with respect to time
x,y,xy = with respect to x-y system (Fig. 2)
0 = prebuckling quantity
1,2 = meridional, circumferential directions
12 = shear, twist

Superscripts

T = transpose, thermal effect
+,− = meridional discontinuity (Fig. 3)
$(\ )^{\cdot}$ = differentiation with respect to θ
$(\ )'$ = differentiation with respect to arc length s
* = axial, radial system (u^*,w^*, for example; Figs. 2 and 3)

Introduction

DURING the past few years the author has been developing a computer program for the general analysis of complex shells of revolution. A series of papers has been published which describe computer programs called BOSOR,

Presented as paper at the AIAA/ASME 11th Structures, Structural Dynamics, and Materials Conference, Denver, Colo., April 22–24, 1970 (no paper number; published as bound volume); submitted May 18, 1970; revision received August 31, 1970. The author is indebted to R. M. Jones of the Aerospace Corporation, San Bernardino, Calif., for many fruitful discussions about the numerical results. The research on thermal buckling was supported under Contract F04701-68-C-0299, CCO No. P001, by the Space and Missile Systems Organization, Air Force Systems Command, Deputy for Ballistic Missile Reentry System, with T. W. Swartz as technical administrator and D. C. Glenn and R. M. Jones of Aerospace Corporation as principal technical monitors. The development of the BOSOR3 computer code was sponsored in part by SAMSO, Aerospace and in part by the Naval Ship Research and Development Center, Carderock, Maryland, under Contract N00014-67-C-0256, Project SF 013 0302. J. Roderick and R. Jones were the technical monitors for the NSRDC contract.

* Staff Scientist. Member AIAA.

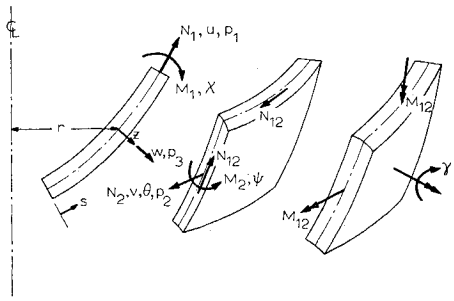

Fig. 1 Shell element with displacements, rotations, forces.

BOSOR 2, and BOSOR 3. These programs represent increasingly improved and more general analyzers for complex shells of revolution; each program in the BOSOR series supersedes the previous programs. The BOSOR 3 code is the latest in the series. The purposes of this paper are to present the analysis on which the BOSOR 3 code is based and to reveal some numerical results involving combined thermal and mechanical loading of ring-stiffened cones and cylinders. The research on thermally loaded cones and cylinders was motivated by the need for a method of predicting buckling loads for re-entry body type shells submitted to combined temperature and pressure.

Portions of most re-entry vehicles are shell structures. They may be composed of multiple layers of orthotropic material, the properties of which depend on the temperature. The shell may be reinforced by ring stiffeners placed at intervals along the length. During re-entry, a vehicle is subjected to a severe thermal environment as well as dynamic pressure and inertia loads due to deceleration. The combination of thermal stress, stress from the dynamic loads, and degradation of the material properties with increasing temperature may cause material failure, buckling, or a combination of these failure modes.

Large stresses are generated in particular by differential heating rates of shell and ring stiffeners. During the initial phase of re-entry the shell heats up rapidly whereas the rings remain relatively cool. Later on, the shell may cool faster than the rings, thereby causing a reversal of the thermal stresses and possible low-cycle fatigue failure. Buckling of the shell in the neighborhood of the rings can occur if the skin heats up before the rings. The cool rings prevent the shell from expanding locally, and the resulting hoop compression in the shell may cause it to buckle. In the reverse situation, shell cool and rings hot, the shell prevents the rings from expanding, thereby giving rise to hoop compression in the rings, which could initiate general instability of skin and rings together.

In the light of the preceding comments, any analysis of a re-entry body for stress and stability should include the effects of material expansion, temperature dependence of the material properties, and discrete ring stiffeners. Since the temperature will sometimes vary rapidly through the thickness of the re-entry vehicle shell, the analysis must permit variation of wall properties through the thickness. These properties must be calculated for each temperature distribution. In the BOSOR 3 program integrated shell wall stiffness coefficients are obtained by interpolation from stored tables of temperature-dependent material properties.

To date, most of the work in thermal buckling applies to isotropic cylindrical shells with temperature-independent material properties. Hoff[1] has clearly discussed the various aspects of the thermal buckling problem from the points of view of the effect of temperature on the material properties and the effect of creep. Abir and Nardo[2] treat the thermal buckling problem for cylinders under circumferential temperature gradients. They find that the critical value of the axial compressive thermal stress does not differ much from the critical stress when the cylinder is subjected to uniform axial compression, provided the variation of the intensity of the thermal stress within one-half wavelength of the buckle pattern is not large. Ross, Hoff, and Horton[3] performed experiments to determine the buckling behavior of uniformly heated thin cylinders clamped at the edges. They determined that for their specimens the buckling stresses are the same whether the loading is thermal or mechanical. Thermal buckling of conical shells has been studied with linear theory by Lu and Chang in Ref. 4 and with nonlinear theory by Chang and Lu in Ref. 5. The material properties are taken to be independent of the temperature in their analyses. Nonlinearities arise from large deflections rather than from temperature dependence of material properties.

A number of papers has been written on the thermal buckling of ring-stiffened cylinders. Hoff[6] calculates buckling loads for cylinders under hoop stresses which vary in the axial direction. These hoop stresses could represent thermal stresses in cylinders with discrete ring stiffeners which are at a lower temperature then that of the shell wall. Hoff gives an example involving a simply supported, uniformly heated cylinder. Anderson[7] and Johns[8] review theoretical and experimental investigations of the buckling of ring-stiffened cylinders due to both axial and circumferential thermal stresses. In all of these analyses, it is assumed that the shell is hot and the rings are cold. There is apparently no analysis for the reverse case—cold shell, hot rings.

Thermal expansion effects are included in computer programs for the analysis of general shells of revolution written by Cohen,[9] Kalnins,[10] and Witmer et al.[11] Temperature-dependence of material properties is not included in these analyses; however, Stern[12] has written a computer program for calculation of stresses and displacements in elastic-plastic shells of revolution with temperature-dependent properties. He does not include discrete ring stiffeners nor perform a buckling analysis.

The present analysis forms the basis of a computer program called BOSOR 3 for the calculation of stress, stability, and vibration of segmented, ring-stiffened shells of revolution with temperature-dependent material properties. This program is documented in Ref. 13. In this paper the general analysis is given, and numerical results are presented which apply to ring-stiffened shells submitted to combined mechanical and thermal loads.

Analysis

Introduction

The BOSOR 3 program[13] represents the codification of three distinct analyses: 1) a nonlinear stress analysis for axisymmetric behavior of axisymmetric shell systems, 2) a linear stress analysis for axisymmetric and nonsymmetric behavior of axisymmetric shell systems submitted to axisymmetric and nonsymmetric loads, and 3) an eigenvalue analysis in which the eigenvalues represent buckling loads or vibration frequencies of axisymmetric shell systems submitted to axisymmetric loads. (Eigenvectors may correspond to axisymmetric or nonsymmetric modes.)

An energy formulation is used in conjunction with the method of finite differences. An algebraic form for the total potential and kinetic energy of the system is derived through extensive use of matrix algebra. The development is similar to that used in the finite element method and is ideally suited for programing on the digital computer. Other investigators[14–17] have also based their analyses on energy minimization in which the displacement derivatives appearing in the kinematic relations are replaced by appropriate finite difference forms. The principal advantages for use of finite differences with energy minimization rather than equilibrium equations are ease of programing of cases involving complex

geometries and symmetry of matrices of coefficients of governing equations.

The independent variables of the analysis are the arc length s measured along the shell reference surface and the circumferential coordinate θ (Fig. 1). The dependent variables are the displacement components u, v, and w of the shell wall reference surface. The numerical analysis is based on the finite-difference method, so that in the computer program the dependent variables are the displacement components u_i, v_i, and w_i at discrete points (mesh points) on the shell reference surface.

For the three analyses just listed, it is possible to eliminate the circumferential coordinate θ by separation of variables: in the nonlinear stress analysis, θ is not present; in the linear stress analysis, the nonsymmetric load system is expressed as a sum of harmonically varying quantities, the shell response to each harmonic being calculated separately; and in the eigenvalue analysis the eigenvectors vary harmonically around the circumference. Thus, the θ dependence (where applicable) is eliminated by the assumption that $u(s,\theta)$, $v(s,\theta)$, $w(s,\theta)$ are given by $u_n(s)\ \sin n\theta$, $v_n(s)\ \cos n\theta$, $w_n(s)\ \sin n\theta$, or by $u_n(s)\ \cos n\theta$, $v_n(s)\ \sin n\theta$, $w_n(s)\ \cos n\theta$. In the following analysis, the first three harmonically varying displacement components correspond to values $n > 0$; the last three to $n \leq 0$.

The advantages of being able to eliminate one of the independent variables cannot be overemphasized. The number of calculations performed by the computer for a given mesh point spacing along the arc length s is greatly reduced, leading to significant reductions in computer time. Because the numerical analysis is "one-dimensional" a rather elaborate composite shell structure can be analyzed in a single "pass" through the computer. The disadvantage is, of course, the restriction to axisymmetric structures.

Energy Formulation

The analysis is based on energy minimization with constraint conditions. The total energy of the system involves 1) strain energy of the shell segments U_s, 2) strain energy of the discrete rings U_r, 3) potential energy of the applied line loads and pressures U_p, 4) kinetic energy of the shell segments T_s, and 5) kinetic energy of the discrete rings T_r. The constraint conditions U_c arise from 1) displacement conditions at the ends of the composite shell, and 2) compatibility conditions between adjacent segments of the composite shell.

These components of energy and the constraint conditions are initially integro-differential forms. They are then written in terms of the shell reference surface displacement components u_i, v_i, and w_i at the finite-difference mesh points and Lagrange multipliers λ_i. The integration is performed numerically by the trapezoidal rule. Now an algebraic form, the energy is minimized with respect to the discrete dependent variables.

In the nonlinear stress analysis the energy expression has terms linear, quadratic, cubic, and quartic in the dependent variables. The cubic and quartic terms arise from the "rotation-squared" terms which appear in the constraint conditions and in the kinematic expressions for reference surface strains ϵ_1, ϵ_2, and ϵ_{12}. Nonlinear material properties (plasticity) are not included in the analysis. Energy minimization leads to a set of nonlinear algebraic equations which are solved by the Newton-Raphson method. Stress and moment resultants are calculated in a straightforward manner from the mesh point displacement components through the constitutive equations (stress-strain law) and kinematic (strain-displacement) relations.

The results from the nonlinear axisymmetric stress analysis are used in the eigenvalue analyses for buckling and vibration. The "prebuckling" or "prestress" meridional and circumferential stress resultants N_{10} and N_{20} and the meridional rotation χ_0 appear as known variable coefficients in the energy expression which governs buckling and vibration. This expression is a homogeneous quadratic form. The values of a parameter (load or frequency) which render the quadratic form stationary with respect to infinitesimal variations of the dependent variables represent buckling loads or natural frequencies. These "eigenvalues" are calculated from a set of linear, homogeneous equations.

The same linear "stability" equations, with a "right-hand-side" vector added, are used for the linear stress analysis of axisymmetrically and nonsymmetrically loaded shells. The "right-hand-side" vector represents load terms and terms due to thermal stress. The variable coefficients N_{10}, N_{20}, and χ_0 mentioned above are zero, of course, since there is no nonlinear "prestress" analysis.

Energy Components and Constraint Conditions

The various components of the energy (U_s, U_r, U_p, T_s, T_r) and the constraint conditions U_c are derived in this section. Variable names are defined in the nomenclature. The energy is derived for a typical shell segment and for a typical discrete ring. The total energy is obtained by summation over all shell segments and all discrete rings.

Shell strain energy

A shell segment is shown in Fig. 1. The strain energy in the shell wall is

$$U_s = \tfrac{1}{2}\int_s\int_\theta\int_z \{\sigma_1(\mathcal{E}_1 - \alpha_1 T) + \sigma_2(\mathcal{E}_2 - \alpha_2 T) + \tau_{12}\mathcal{E}_{12}\} r\,dz\,d\theta\,ds \tag{1}$$

for an orthotropic wall

$$\begin{Bmatrix}\sigma_1\\ \sigma_2\\ \tau_{12}\end{Bmatrix} = \begin{bmatrix}E_{11} & E_{12} & 0\\ E_{12} & E_{22} & 0\\ 0 & 0 & G\end{bmatrix}\begin{Bmatrix}\mathcal{E}_1 - \alpha_1 T\\ \mathcal{E}_2 - \alpha_2 T\\ \mathcal{E}_{12}\end{Bmatrix} \tag{2}$$

If "normals remain normal" and undeformed (a classical thin shell theory approximation), the strains as functions of the thickness $\mathcal{E}_1(z)$, $\mathcal{E}_2(z)$, and $\mathcal{E}_{12}(z)$ can be expressed in terms of reference surface strains ϵ_1, ϵ_2, and ϵ_{12} and changes in curvature κ_1, κ_2, and κ_{12}, thus

$$\mathcal{E}_1 = \epsilon_1 - z\kappa_1, \quad \mathcal{E}_2 = \epsilon_2 - z\kappa_2, \quad \mathcal{E}_{12} = \epsilon_{12} + 2z\kappa_{12} \tag{3}$$

It is convenient to perform the z integration in Eq. (1) at this point. The following definitions of stress and moment resultants are required:

$$N_1 = \int\sigma_1 dz \quad N_2 = \int\sigma_2 dz \quad N_{12} = \int\tau_{12} dz \tag{4a}$$

$$M_1 = -\int\sigma_1 z\,dz \quad M_2 = -\int\sigma_2 z\,dz \quad M_{12} = \int\tau_{12} z\,dz \tag{4b}$$

These stress and moment resultants are shown in Fig. 1. Substitution of Eqs. (2) with Eqs. (3) into Eqs. (4) gives:

$$\begin{Bmatrix}N_1\\ N_2\\ N_{12}\\ M_1\\ M_2\\ M_{12}\end{Bmatrix} = \begin{bmatrix}C_{11} & C_{12} & 0 & C_{14} & C_{15} & 0\\ C_{12} & C_{22} & 0 & C_{24} & C_{25} & 0\\ 0 & 0 & C_{33} & 0 & 0 & C_{36}\\ C_{14} & C_{24} & 0 & C_{44} & C_{45} & 0\\ C_{15} & C_{25} & 0 & C_{45} & C_{55} & 0\\ 0 & 0 & C_{36} & 0 & 0 & C_{66}\end{bmatrix} \times \begin{Bmatrix}\epsilon_1\\ \epsilon_2\\ \epsilon_{12}\\ \kappa_1\\ \kappa_2\\ 2\kappa_{12}\end{Bmatrix} + \begin{Bmatrix}N_1^T\\ N_2^T\\ 0\\ M_1^T\\ M_2^T\\ 0\end{Bmatrix} \tag{5}$$

in which

$$C_{11} = \int E_{11} dz \quad C_{12} = \int E_{12} dz \quad C_{14} = -\int E_{11} z\,dz \tag{6a}$$

$$C_{15} = -\int E_{12} z\,dz \quad C_{22} = \int E_{22} dz \quad C_{24} = -\int E_{12} z\,dz \tag{6b}$$

$$C_{25} = -\int E_{22} z\,dz \quad C_{33} = \int G\,dz \quad C_{36} = \int G z\,dz \tag{6c}$$

$$C_{66} = \int G z^2 dz \quad C_{44} = \int E_{11} z^2 dz \quad C_{45} = \int E_{12} z^2 dz \tag{6d}$$

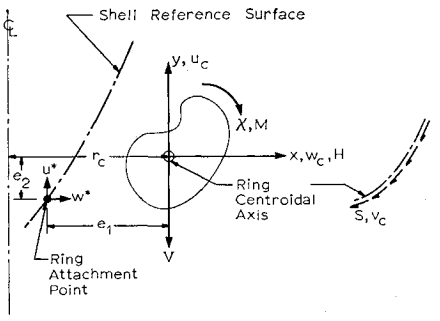

Fig. 2 Discrete ring with centroidal displacements, forces.

$$C_{55} = \int E_{22}z^2dz \quad N_1{}^T = -\int(E_{11}\alpha_1 T + E_{12}\alpha_2 T)dz \tag{6e}$$

$$N_2{}^T = -\int(E_{12}\alpha_1 T + E_{22}\alpha_2 T)dz \tag{6f}$$

$$M_1{}^T = \int(E_{11}\alpha_1 T + E_{12}\alpha_2 T)zdz \tag{6g}$$

$$M_2{}^T = \int(E_{12}\alpha_1 T + E_{22}\alpha_2 T)zdz \tag{6h}$$

The thickness coordinate z is measured from the reference surface outward. The integrations through the thickness in Eqs. (6) can be performed explicitly for layered shells with material properties constant through the thickness of each layer, or numerical integration can be performed (e.g., Simpson's rule) for layered shells with temperature-dependent material properties. In BOSOR 3 a program branch is provided in which the C_{ij} are calculated from numerical integration in which the integrands are machine-derived by means of automated interpolation of "raw" tabular input data $E_1(i,T)$, $E_2(i,T)$, $\nu_{12}(i,T)$, $G(i,T)$, $\alpha_1(i,T)$, $\alpha_2(i,T)$, i = one to maximum number of layers of shell wall. The shell energy U_s in Eq. (1) can now be written in the form

$$U_s = \tfrac{1}{2}\int_s\int_\theta [[S]\{\epsilon\} + [N^T]\{\epsilon\} + C(T)]rd\theta ds \tag{7}$$

in which

$$[S] \equiv [N_1,N_2,N_{12},M_1,M_2,M_{12}], \quad \{\epsilon\} = [\epsilon]^T \equiv$$
$$[\epsilon_1,\epsilon_2,\epsilon_{12},\kappa_1,\kappa_2,2\kappa_{12}]^T \quad [N^T] \equiv [N_1{}^T,N_2{}^T,0,M_1{}^T,M_2{}^T,0]$$

and $C(T)$ is a function of the shell parameters and temperature rise only. Therefore it can be dropped. Since

$$[S] = \{S\}^T = [[C]\{\epsilon\} + \{N^T\}]^T \tag{8a}$$

$$= [\epsilon][C]^T + [N^T] \tag{8b}$$

$$= [\epsilon][C] + [N^T] \tag{8c}$$

substitution of Eq. (8) for $[S]$ and the dropping of $C(T)$ in Eq. (7) leads to

$$U_s = \tfrac{1}{2}\int_s\int_\theta [[\epsilon][C]\{\epsilon\} + 2[N^T]\{\epsilon\}]rd\theta ds \tag{9}$$

The strain-displacement relations are

$$\left\{\epsilon\right\} = \begin{Bmatrix} \epsilon_1 \\ \epsilon_2 \\ \epsilon_{12} \\ \kappa_1 \\ \kappa_2 \\ 2\kappa_{12} \end{Bmatrix} = \begin{matrix} u' + w/R_1 + \tfrac{1}{2}(\chi^2 + \gamma^2) \\ \dot{v}/r + ur'/r + w/R_2 + \tfrac{1}{2}(\psi^2 + \gamma^2) \\ \dot{u}/r + r(v/r)' + \chi\psi \\ \chi' \\ \dot{\psi}/r + r'\chi/r \\ 2(-\dot{\chi}/r + r'\psi/r + v'/R_2) \end{matrix} \tag{10}$$

in which

$$\chi = w' - u/R_1, \; \psi = \dot{w}/r - v/R_2 \tag{11a}$$

$$\gamma = \tfrac{1}{2}(\dot{u}/r - v' - r'v/r) \tag{11b}$$

Dots indicate differentiation with respect to θ; primes indicate differentiation with respect to s. Positive values of u, v, w, χ, ψ, and γ are shown in Fig. 1. The quantities R_1 and R_2 are the meridional and normal circumferential radii of curvature.

Discrete ring strain energy

Figure 2 shows a ring cross section with displacements u_c, v_c, w_c, χ of the centroid and applied loads V, S, H, M. The centroid and the shear center are assumed to coincide and plane normal sections are assumed to remain plane and normal during deformations. In the absence of warping, the ring strain energy is given by

$$U_r = (r_c/2)\int_\theta\int_A \sigma_r(\mathcal{E}_r - \alpha_r T)dAd\theta + \tfrac{1}{2}(GJ/r_c)\int_\theta(\dot{\chi} + \dot{u}_c/r_c)^2d\theta \tag{12}$$

The ring hoop stress is given by

$$\sigma_r = E_r(\mathcal{E}_r - \alpha_r T) \tag{13}$$

The hoop strain $\mathcal{E}_r$ can be expressed as a function of strain of the centroidal axis plus terms due to in-plane and out-of-plane curvature changes κ_x and κ_y, respectively:

$$\mathcal{E}_r = \epsilon_r - x\kappa_x + y\kappa_y \tag{14}$$

Substitution of Eqs. (14) and (13) into Eq. (12), integration over the ring area, and the dropping of the term which contains only ring parameters and temperature, leads to the following expression for the ring energy:

$$U_r = (r_c/2)\int_\theta \{\epsilon_r{}^2EA + \kappa_x{}^2EI_y + \kappa_y{}^2EI_x - 2\kappa_x\kappa_yEI_{xy} + (GJ/r_c{}^2)(\dot{\chi} + \dot{u}_c/r_c)^2 + 2[\epsilon_rN_r{}^T - \kappa_xM_y{}^T + \kappa_yM_x{}^T]\}d\theta \tag{15}$$

in which

$$N_r{}^T = -\int E_r\alpha_r TdA \tag{16a}$$

$$M_y{}^T = -\int E_r\alpha_r Txd A \quad M_x{}^T = -\int E_r\alpha_r Tyd A \tag{16b}$$

and the ring kinematic relations are

$$\epsilon_r = \dot{v}_c/r_c + w_c/r_c + \tfrac{1}{2}(\psi_c{}^2 + \gamma_c{}^2) \tag{17a}$$

$$\kappa_x = \dot{\psi}_c/r_c \tag{17b}$$

$$\kappa_y = -\dot{\gamma}_c/r_c + \chi/r_c \tag{17c}$$

$$\psi_c = (\dot{w}_c - v_c)/r_c \tag{17d}$$

$$\gamma_c = \dot{u}_c/r_c \tag{17e}$$

Potential energy of mechanical loads

Two types of loads are permitted in the analysis: line loads and moments V, S, H, and M, which act at ring centroids and at shell segment boundaries, and surface tractions p_1, p_2, and p_3. These loads are shown in Figs. 1 and 2. The potential energy associated with line loads at a given ring station is

$$U_{p1} = -\int_\theta(-Vu_c + Sv_c + Hw_c + M\chi)r_cd\theta \tag{18}$$

The potential energy associated with the surface tractions is

$$U_{p2} = -\int_s\int_\theta(p_1u + p_2v + p_3w)rd\theta ds \tag{19}$$

Kinetic energy of shell segment

The kinetic energy of the shell segment is given by

$$T_s = \tfrac{1}{2}\int_s\int_\theta m(u,_t{}^2 + v,_t{}^2 + w,_t{}^2)rd\theta ds \tag{20}$$

in which $(\;),t$ denotes differentiation with respect to time. The shell rotatory inertia is neglected.

Kinetic energy of discrete ring

The kinetic energy of a discrete ring stiffener is given by

$$T_r = \rho_r(r_c/2)\int_\theta[A(u_{c,t}{}^2 + v_{c,t}{}^2 + w_{c,t}{}^2) + I_p\chi,_t{}^2 + I_s\psi_{c,t}{}^2 + I_n\gamma_{c,t}{}^2 - 2I_{sn}\psi_{c,t}\gamma_{c,t}]d\theta \tag{21}$$

in which I_p, I_s, I_n, I_{sn} are cross-sectional area moments of inertia relative to axes normal and tangential to the shell meridian at the ring attachment point. In the case of harmonic oscillations, the differentiations with respect to time are replaced by a factor Ω, which is a frequency parameter.

Constraint conditions

Figure 3 shows a meridional discontinuity between two adjacent shell segment reference surfaces (3a) and discontinuities at shell edge support points "A" and "B" (3b). The compatibility conditions for the juncture are

$$u^{*+} = u^{*-} + \Delta u^* \qquad v^{*+} = v^{*-} + \Delta v^* \tag{22a}$$

$$w^{*+} = w^{*-} + \Delta w^* \qquad \chi^+ = \chi^- \tag{22b}$$

in which

$$\Delta u^* = -(d_1\chi + d_2\chi^2/2) \tag{23a}$$

$$\Delta v^* = -(d_1 + \Delta w^*)(\dot{w}^{*-} - v^{*-})/r^- - (d_2+\Delta u^*)\dot{u}^{*-}/r^- \tag{23b}$$

$$\Delta w^* = d_2\chi - d_1\chi^2/2 \tag{23c}$$

The constraint conditions (22) arise from the requirement that the motion of point D relative to point C (Fig. 3) involves no deformation of a line joining C and D and continuous rotation χ. At a support point the terms u^{*+}, v^{*+}, and w^{*+} in Eqs. (22) are zero if the appropriate boundary condition integers $KA1$, $KA2$, etc., and $KB1$, $KB2$, etc. (see below), are equal to unity. The constraint conditions (22) are incorporated into the total system energy by the introduction of four Lagrange multipliers λ_1, λ_2, λ_3, and λ_4 for each edge support and each segment juncture. Thus, the "energy of constraint" corresponding to each juncture has the form

$$U_c = [\lambda_1,\lambda_2,\lambda_3,\lambda_4]\begin{Bmatrix} u^{*+} - u^{*-} - \Delta u^* \\ v^{*+} - v^{*-} - \Delta v^* \\ w^{*+} - w^{*-} - \Delta w^* \\ \chi^+ - \chi^- \end{Bmatrix} \tag{24}$$

At the shell ends the constraint conditions have the following forms: at "A"

$$U_c = [KA1^*\lambda_1, KA2^*\lambda_2, KA3^*\lambda_3, KA4^*\lambda_4]\begin{Bmatrix} -u^{*-} - \Delta u^* \\ -v^{*-} - \Delta v^* \\ -w^{*-} - \Delta w^* \\ -\chi^- \end{Bmatrix}$$

at "B"

$$U_c = [KB1^*\lambda_1, KB2^*\lambda_2, KB3^*\lambda_3, KB4^*\lambda_4]\begin{Bmatrix} -u^{*-} - \Delta u^* \\ -v^{*-} - \Delta v^* \\ -w^{*-} - \Delta w^* \\ -\chi \end{Bmatrix} \tag{25}$$

Variable Transformations

The components of energy of the system are represented by the shell strain energy U_s [Eq. (9)], the strain energy of a discrete ring U_r [Eq. (15)], the potential energy of line loads U_{p1} and surface tractions U_{p2} [Eqs. (18) and (19)], the shell kinetic energy T_s [Eq. (20)], and the discrete ring kinetic energy T_r [Eq. (21)]. The constraint conditions U_c are given by Eqs. (24) and (25).

It is desired to express all energy components in terms of the shell reference displacements u, v, and w. The displacements u_c, v_c, and w_c of the ring centroid (Fig. 2), which appear in Eqs. (15, 17, 18, and 21), are given by

$$u_c = u^* + \Delta u^* \quad v_c = v^* + \Delta v^* \quad w_c = w^* + \Delta w^* \tag{26}$$

The quantities Δu^*, Δv^*, and Δw^* are given by Eqs. (23) with d_1 and d_2 replaced by e_1 and e_2, the ring eccentricity components (Fig. 2), and u^{*-}, v^{*-}, w^{*-}, r^- replaced by the displacement components and radius u^*, v^*, w^*, r which correspond to the ring attachment point. The axial, circumferential, and radial displacement components u^*, v^*, and w^*, which appear in Eqs. (22–26), are given by

$$u^* = ur/R_2 - wr' \quad v^* = v \quad w^* = ur' + wr/R_2 \tag{27}$$

Equations (26) and (27) can be used to eliminate u_c, v_c, w_c, u^*, v^*, and w^* from the energy components and constraint conditions. The dependent variables are then u, v, w and the Lagrange multipliers λ_1, λ_2, λ_3, and λ_4.

The total energy in the system is obtained by summing over all shell segments, discrete ring stiffeners, and junctures.

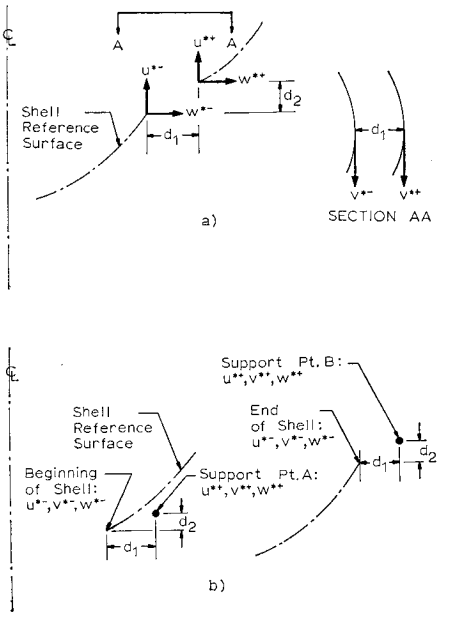

Fig. 3 Geometry for constraint conditions: a) Shell reference surface discontinuity, b) support points.

Separation of Variables

The dependent variables u, v, and w are functions of arc length s and circumferential coordinate θ. The θ dependence can be eliminated from the analysis by the assumption that

$$u(s,\theta) = u_0(s) + \sum_{n=n_{\min}}^{n_{\max}} u_{n1}(s)\sin n\theta + \sum_{n_{\min}}^{n_{\max}} u_{n2}(s)\cos n\theta$$

$$v(s,\theta) = \sum_n v_{n1}(s)\cos n\theta + \sum_n v_{n2}(s)\sin n\theta \tag{28}$$

$$w(s,\theta) = w_0(s) + \sum_n w_{n1}(s)\sin n\theta + \sum_n w_{n2}(s)\cos n\theta$$

The temperature distribution, surface tractions and pressures, and thermal and mechanical line loads have similar expansions, which are given explicitly in Ref. 18.

If the expressions (28) were inserted into the energy components just derived, all the harmonics would couple in the analysis, since the kinematic relations (10, 17, and 23) are nonlinear.

In the analysis, large deflections are permitted in the axisymmetric components, but the nonsymmetric harmonics are considered to be small. The various harmonics do not couple, and a solution for each $u_n(s)$, $v_n(s)$, and $w_n(s)$ can be obtained with the circumferential wave number n appearing as a parameter in the analysis. The θ integration indicated in Eqs. (9, 15, and 18–21) is replaced by a factor of π for $n \neq 0$ and 2π for $n = 0$. In a linear stress analysis for nonsymmetrically loaded shells, the static response of a shell to

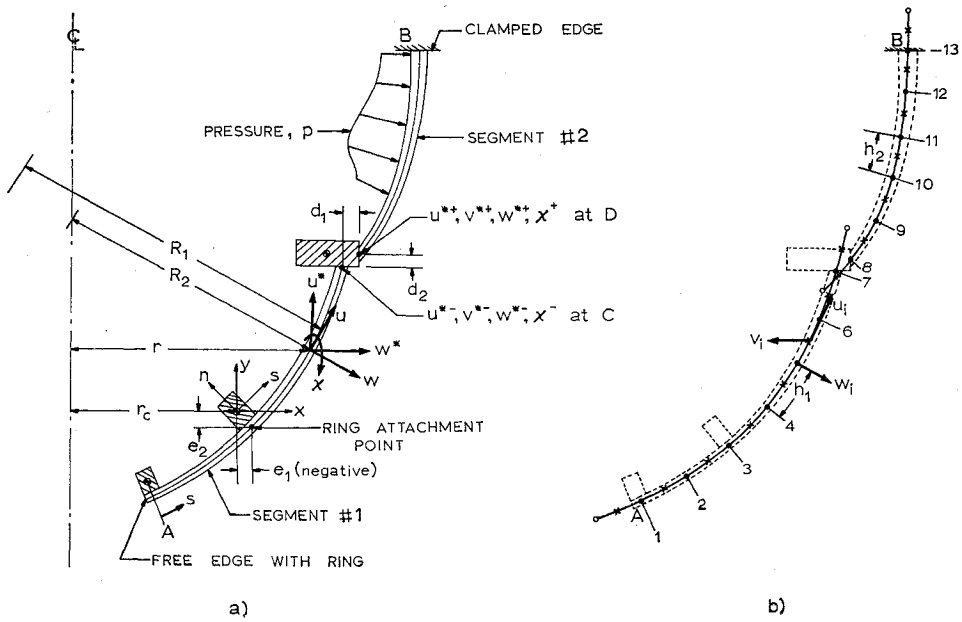

Fig. 4 Shell meridian with finite-difference model: a) shell with two segments, b) finite-difference model.

arbitrarily varying loads is obtained by superposition. (In this case, even the axisymmetric components are assumed to be small.) In buckling and vibration analyses the "small" deflections u_{n1}, v_{n1}, w_{n1}, u_{n2}, v_{n2}, w_{n2} are considered to be kinematically admissible variations from the "prebuckled" or "prestressed" axisymmetric state represented by the large deflections $u_0(s)$ and $w_0(s)$ in Eqs. (28). The $u_0(s)$ and $w_0(s)$ are determined in the nonlinear stress analysis portion of the analysis.

In the linear analysis for nonsymmetric behavior and in the buckling and vibration analyses, the second summations in Eqs. (28) can be represented by negative values of the wave number n. Positive values of n correspond to the first summations. In the remainder of this section the subscripts $(\ )_{n1}$ and $(\ )_{n2}$ will be dropped. It is emphasized that the analysis and computer program are valid for negative values of n.

Finite Difference Scheme

The θ dependence has been replaced with a parameter n, so that only one independent variable remains—the arc length s. Figure 4a shows a shell meridian of two segments, and Fig. 4b shows the finite-difference model. The continuous variables $u(s)$, $v(s)$, and $w(s)$ are replaced by discrete variables u_i, v_i, and w_i. The u_i and v_i occur at stations midway between the w_i. This arrangement of discrete variables has been determined to be superior to an arrangement in which u_i, v_i, and w_i correspond to displacement components at a single point. Detailed comparisons between the two schemes are given in Ref. 19. The energy is evaluated at the mesh points where the w_i are located. The displacements and the s derivatives required in the energy are

$$u = (u_i + u_{i-1})/2, \quad v = (v_i + v_{i-1})/2 \tag{29a}$$

$$u' = (u_i - u_{i-1})/h, \quad v' = (v_i - v_{i-1})/h \tag{29b}$$

$$w = w_i, \quad w' = (w_{i+1} - w_{i-1})/2h,$$

$$w'' = (w_{i+1} - 2w_i + w_{i-1})/h^2 \tag{29c}$$

in which h is the mesh point spacing.

The s integration indicated in Eqs. (9, 19, and 20) is performed numerically by the trapezoidal rule.

With the substitution of Eqs. (28) in the various energy components and constraint conditions, the replacement of s derivatives by Eqs. (29), the replacement of time derivatives by a frequency parameter, and the numerical integration over s and exact integration over θ, the system energy and constraint conditions are now represented by an algebraic form which contains as dependent variables u_i, v_i, and w_i and the Lagrange multipliers λ_1, λ_2, λ_3, and λ_4 (for each juncture and boundary). The algebraic form also contains as parameters the shell and ring properties, the loads and temperature, and the frequency parameter Ω.

Stress, Buckling, and Vibration Analyses

In the nonlinear stress analysis only the axisymmetric components of the load are considered and only $u_0(s)$ and $w_0(s)$ in Eqs. (28) are nonzero. Terms linear through quartic appear in the algebraic form for the total energy. The simultaneous nonlinear algebraic equations obtained by energy minimization are solved by the Newton-Raphson method. A complete description appears in Ref. 18. The coefficient matrix for each iteration is symmetric and is strongly banded about the main diagonal. The bandwidth is 9 elements except at shell segment junctures where it is 15. Such narrowly banded systems can be solved in a matter of seconds of computer time. For example, a case with 225 degrees of freedom requires somewhat less than about 2 sec per iteration with double precision on the UNIVAC 1108 computer. The number of iterations required depends on how nonlinear the problem is. Generally, less than about five iterations are needed for convergence at a given load level.

In the computer program BOSOR 3 (see Ref. 13), the convergence criterion is that successive values of all u_{i0}, w_{i0} greater than a tenth of the largest displacement be different by less than 0.1% of their absolute values. The starting vector for the first iteration and the first load value is zero, which means that the first solution represents the linear theory solution. The starting vectors for the first iterations at subsequent load values are the converged solutions obtained at the loads immediately preceding the current load. Once the displacements u_{i0} and w_{i0} have been calculated, the stresses are obtained in a straightforward manner by means of Eqs. (10) and (5).

In the buckling and vibration analyses the symmetric and nonsymmetric displacement components contained in the summations indicated in Eq. (28) are considered to be infinitesimal, kinematically admissible variations of the displacements from the "prebuckled" or "prestressed" state obtained in the nonlinear stress analysis described above. Since the "buckling" displacements u_n, v_n, and w_n are in-

finitesimal, one need only retain linear terms in u_n, v_n and w_n in the kinematic relations and constraint conditions. However, it must be remembered that the displacements and rotations in Eqs. (10–26) represent the total displacements from the undeformed state. Hence, cross-product terms such as $w_0 w_n$ obtained by insertion of Eqs. (28) [with the use of Eqs. (11a) and (29)] into Eqs. (10), for example, must be retained. The energy minimization in the buckling and vibration analyses is performed with respect to u_n, v_n, w_n and the Lagrange multipliers. The prebuckling quantities u_0 and w_0 do not vary during buckling or vibration but are simply parameters of the shell system.

The buckling and vibration analysis is described in detail in Ref. 19, and this description will not be repeated here. It is sufficient to point out that the energy expression on which the numerical analysis is based is a homogeneous quadratic form. The form is stationary with respect to the dependent variables u, v, w and the Lagrange multipliers λ for certain discrete values of a parameter—the so-called eigenvalues. In the BOSOR 3 program the eigenvalue parameter can be a load or load ratio, a temperature, or a frequency.

The linear stress analysis is based on the same equations as the stability and vibration analysis, except that the "prestress" terms which appear in the stability and vibration quadratic form are not present, and the energy functional is not homogeneous, since a "right-hand-side" vector is nonzero. This vector arises from the thermal terms in Eqs. (9) and (15) and the load terms in Eqs. (18) and (19). The thermal and mechanical loads are distributed circumferentially as given in Eqs. (29) of Ref. 18.

Numerical Results

The BOSOR 3 computer program,[13] which is based on the above analysis, was used to calculate stresses and buckling loads for ring-stiffened shells submitted to mechanical and thermal loads.

Simply-Supported Cylinder

One of the test cases for checking the BOSOR 3 program involved buckling of a simply supported cylinder (N_1, v, w, $M_1 = 0$ at both ends) subjected to a uniform temperature rise. Buckling, if any, is caused by the hoop compressive stresses which exist in the "boundary layers" near the end supports of the heated cylinder. There is no prebuckling axial compression, since the cylinder is free to expand in the axial direction. The cylinder geometry and material properties are those assumed by Hoff in Ref. 6: $E = 29 \times 10^6$ psi, $\nu = 0.3$, $\alpha = 7.2414 \times 10^{-6}$/°F, length = 3.14 in., radius = 10.0 in., and thickness = 0.0331 in. The following results were obtained:

1) With prebuckling rotations χ_0 and rotations-squared χ_0^2 neglected in the stability analysis, good agreement is obtained with the results presented in Ref. 6 with the same simplifications. The prebuckling hoop stress distribution agrees very well with that of Ref. 6, as well as the buckling temperature and corresponding circumferential wave number ($T_{crit} = 2400$°F, $n = 35$).

2) With prebuckling rotations χ_0 included, but rotations-squared χ_0^2 neglected in the stability analysis, the calculated T_{crit} is 410°F with $n = 28$ circumferential waves.

3) With linear and quadratic terms in prebuckling rotations χ_0 included in the stability analysis, it is concluded from the calculations that there is no buckling under the conditions set forth above. For increasing values of temperature, the stability determinant increases monotonically without any change in sign.

Because of these rather unexpected results, the author asked Fulton[20] and Cohen[21] to run this case with their computer programs for the three types of approximations enumerated above. The same results were obtained in all cases. It appears that the calculated buckling temperatures are particularly sensitive to prebuckling meridional rotations because these rotations assume their maximum values in the same regions where the destabilizing hoop compression is large—near the edges of the cylinder. It appears probable that the failure of BOSOR 3 to predict buckling in this case is caused by the restriction of the theory to "moderate" prebuckling rotations.

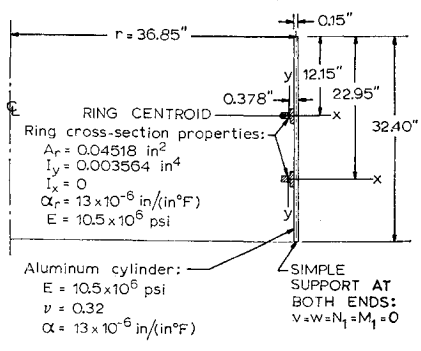

Fig. 5 Ring-stiffened cylinder.

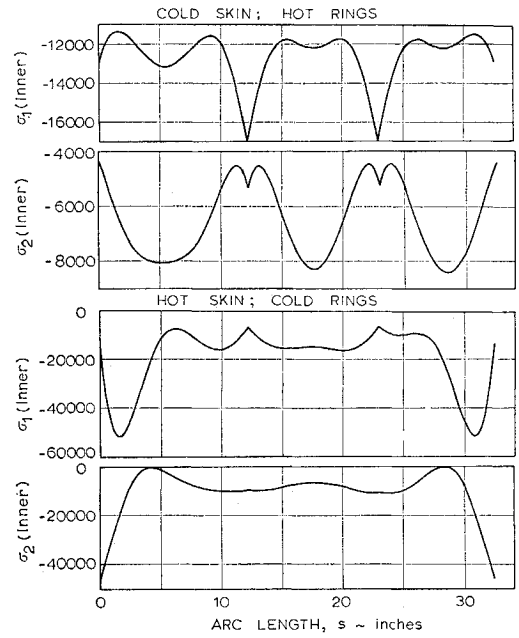

Fig. 6 Inner fiber stresses for external pressure $p = 30$ psi and axial compression $N_1 = 2047$ lb/in.; skin or rings at 300°F; cylinder shown in Fig. 5.

Simply-Supported, Ring-Stiffened Cylinder

Figure 5 shows a ring-stiffened aluminum cylinder, simply supported at the ends. The cylinder is submitted to axial compression, external pressure, and various temperature distributions. The axial compression N_1 and external pressure p are assumed to act proportionally such that $pr/N_1 = 0.54$. The following cases are presented: 1) 300°F temperature rise in skin above zero-stress temperature and rings "cold," 2) 300°F temperature rise in rings and skin "cold," 3) 300°F temperature rise in both rings and skin, and 4) both skin and rings "cold."

Figure 6 shows the inner fiber meridional and circumferential stress distributions for Cases 1 and 2 with the external pressure $p = 30$ psi and axial compression $N_1 = 2047$ lb/in. Notice the high stresses near the simply supported edges due to the radial restraint imposed on the hot shell by the end supports.

Table 1 Buckling loads p for ring-stiffened cylinder with combined axial compression and external pressure such that $pr/N_1 = 0.54$

Circumferential wave number n	Case 1 Skin at 300°, rings cold		Case 2 Skin cold, rings at 300°		Case 3 Skin and rings at 300°		Case 4 Skin and rings cold	
	P_1	P_2	P_1	P_2	P_1	P_2	P_1	P_2
6	56.6	58.8	51.9	58.7	49.8	55.1	54.9	56.8
8	29.7	56.6	26.5	51.9	30.3	53.0	26.5	54.6
10	28.5[a]	47.5	25.0[a]	38.5	28.0[a]	47.4	25.2[a]	38.7
12	32.0	39.7	27.9	31.4	31.2	39.0	28.3	32.1
14	32.5	36.5	26.3	31.0	31.6	36.0	26.7	31.7
16	31.5[a]	36.4[a]	25.9[a]	30.4[a]	30.8[a]	36.0[a]	26.2[a]	30.8[a]
18	32.1	37.4	27.5	31.4	31.7	37.2	27.7	31.6

[a] These values shown in Table 2.

Table 2 Critical buckling loads p corresponding to various modes

Buckling mode	Case 1 Skin hot, rings cold	Case 2 Skin cold, rings hot	Case 3 Skin and rings hot	Case 4 Skin and rings cold
General instability (n = 10 waves)	28.5	25.0	28.0	25.2
First bay predominates (n = 16 waves)	36.4	25.9	36.0	26.2
Second bay predominates (n = 16 waves)	31.5	30.4	30.8	30.8

Tables 1 and 2 and Fig. 7 give buckling loads and mode shapes corresponding to the four cases described previously. In Table 1, two eigenvalues (P_1, P_2) are given for each circumferential wave number. Two eigenvalues were calculated for each n rather than just the lowest in order to obtain a more complete physical understanding of the local buckling phenomenon. Notice that the lowest eigenvalues $P_1(n)$ have two minima with wave number n. The minimum at n = 10 waves corresponds to general instability. The minimum at 16 waves corresponds to either the first or the second bay predominating in the buckling mode, depending on the temperature distribution. (The first bay is nearest the top of the cylinder in Fig. 5.) The eigenvalues correspond in general to three types of buckling: buckling due primarily to the axial component of the load system, general instability due primarily to the pressure, and local instability of the bays between the rings. Typical mode shapes corresponding to these types of buckling are shown in Fig. 7 for Case 4 (cold shell and rings).

The following summary emerges from a study of the data in Tables 1 and 2:

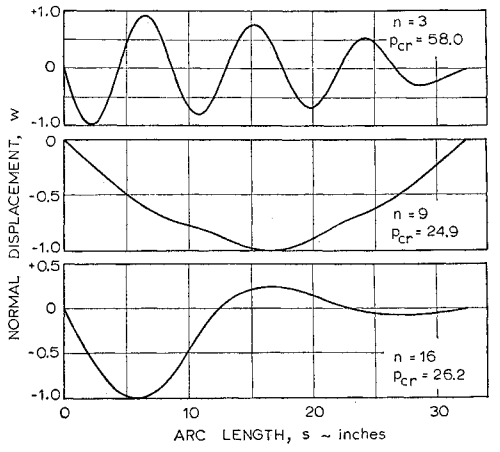

Fig. 7 Buckling mode shapes corresponding to top) axial component of load, center) pressure (general instability), bottom) pressure (local instability of first bay).

1) The critical buckling mode for this geometry and mechanical load combination is general instability, and the critical load system (p, N_1) is not too strongly dependent on the temperature distribution (p_{cr} increased from 25.2 to 28.0 psi when shell is heated).

2) Buckling modes corresponding to local instability (n = 16 waves) depend on the temperature distribution. The most significant effect is the "strengthening" of the first bay due to heating the skin (first bay critical pressure increased from 26.2 psi to 36.0 psi, Table 2).

3) The critical pressure of the second bay (30.4 to 31.5 psi) is almost independent of the temperature distribution.

4) Whether the rings are hot or cold makes little difference for this geometry. The skin temperature is far more important.

The following conclusions can be drawn from the above four observations:

1) The boundary restraints at the ends of the shell cause the most significant changes in buckling behavior with change in temperature distribution.

2) The effect of boundary restraint depends on the length of the shell participating in the buckling deformations. Note that with general instability the effect is relatively small (p_{cr} changes from 25.2 to 28.0 psi), but that with local in-

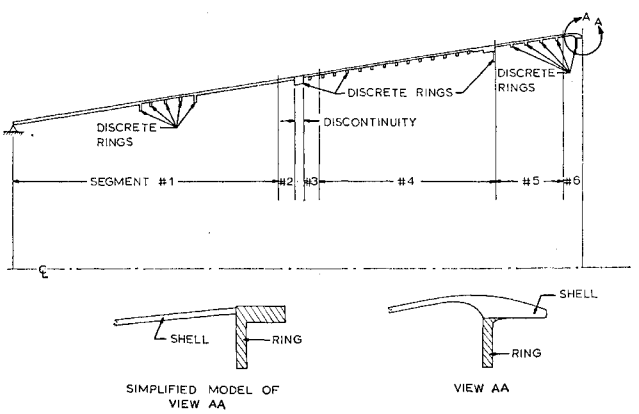

Fig. 8 Ring-stiffened conical shell as analyzed with the BOSOR3 computer program.

Table 3 Buckling pressures in pounds per square inch for ring-stiffened conical shell shown in Fig. 8 (where applicable, temperature difference between skin and rings is 330°F)

Temperature distribution between shell and discrete rings	Analytical model used			
	Actual end	View A-A	Simplified end	View A-A
Cold skin, cold rings	81.8(2)[a]	71.1(6)	44.0(2)	
Hot skin, hot rings	81.8(2)			
Cold skin, hot rings	78.5(2)	70.2(6)		
Hot skin, cold rings	85.7(2)	73.7(6)	58.7(2)	
Cold skin,[b] hot rings	58.1(2)	69.8(6)		
Cold skin,[b] hot rings (Shell assumed to tear at beginning of Segment 3 under prebuckling stresses)	18.4(2)			

[a] Numbers in parentheses are circumferential buckling waves.
[b] Temperature increasing from beginning to end of Segment 6.

stability of the first bay, the effect is rather large (p_{cr} changes from 26.2 to 36.0 psi as the shell is heated).

3) The "stabilizing" effect of prebuckling meridional rotations χ_0 due to heating of the shell is more important in this case than is the "destabilizing" effect of hoop compression in the immediate neighborhood of the edges. When the shell is heated, it "bulges" out. The positive curvature thus created near the end supports serves to strengthen the shell as far as buckling under external pressure is concerned.

Study of Aluminum Ring-Stiffened Conical Shell

Figure 8 shows a ring-stiffened aluminum conical shell which was submitted to external pressure and heated. The integrated pressure was reacted at the small end of the cone. The tests were performed by Avco Corporation.[22] Two tests were conducted, a test involving external pressure only and a test involving both pressure and heating. Without thermal effects, the specimen survived a pressure of 60 psi without any visible damage, but it failed at 34 psi when heated to 400°F. The failure occurred suddenly when the heat sources (lamps) were extinguished.

Two models were analyzed, one in which the large end of the structure (View AA) is shown as "Simplified Model at View AA" and the actual geometry "View AA." The presence of four rather rigid meridional stiffeners in Segments 5 and 6, spaced at 90° around the circumference is neglected in the analysis. This simplification will be justified below.

Figure 9 shows meridional stresses for two temperature distributions in the conical shell with the "simplified" end. The external pressure is 30 psi and the temperature difference between skin and rings is 330°F. The maximum stresses occur at the beginning of Segment 3 adjacent to the large discrete ring there (Fig. 8). These stresses exceed the ultimate stresses in the material, which is aluminum, so that considerable plastic flow occurs prior to buckling at this point. The maximum stresses corresponding to "cold skin, hot rings" (skin at ambient, rings at 330°F above ambient) are somewhat higher than those corresponding to "heated skin, cold rings," since the maximum stresses due to the applied pressure have the same sign in the former case and opposite sign in the latter.

Table 3 gives buckling pressures in psi for both "simplified" and "actual" models shown in Fig. 8. The circumferential wave numbers are given in parentheses. The large differences between the buckling loads for the simplified end A-A and the actual end A-A are presumably due to the positive curvature at the end in the latter case, which serves to increase locally the effective moment of inertia of the skin. The model was changed from "simplified" to "actual" during the

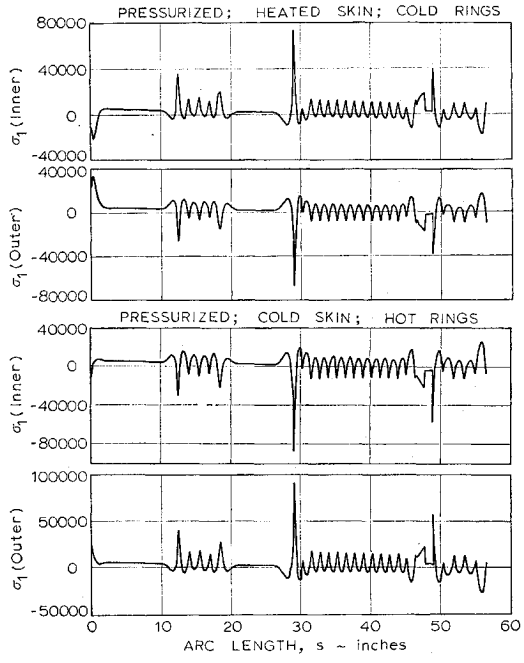

Fig. 9 Meridional stresses in ring-stiffened conical shell submitted to 30 psi external pressure; temperature difference between shell and rings = 300°F.

course of this investigation because the predicted buckling pressure of 44.0 psi (simplified model) with no thermal effects is considerably lower than the pressure applied to the test specimen in the initial phase of the experiment. Both models are shown here in order to demonstrate the sensitivity of the $n = 2$ buckling pressure to small changes in geometry.

Several cases are shown in Table 3. There are two minima with circumferential wave number n, one at $n = 2$ and one at $n = 6$. Typical buckling modes corresponding to these two values of n are shown in Fig. 10. The $n = 2$ modes correspond to general instability of the entire structure. The $n = 6$ mode corresponds to buckling of Segments 3 and 4 (Fig. 8). The omission of the four equally spaced meridional stiffeners in the model of Segments 5 and 6 is justified since the $n = 2$ mode has four w nodes and the $n = 6$ mode does not involve these segments.

The lowest buckling pressure yet predicted for the undamaged model with the "actual" end A-A is 58.08 psi, still above the experimental value of 35 psi. This case is the same as the third case in Table 3 except that a temperature gradient along the reference surface was assumed in Segment 6, temperature increasing toward the large end of the shell. This gradient has the effect of deforming Segment 6 in such a way

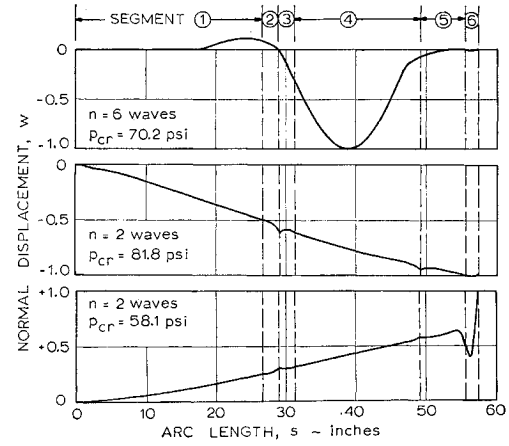

Fig. 10 Buckling modes for $n = 6$ and $n = 2$ circumferential waves for ring-stiffened conical shell shown in Fig. 8.

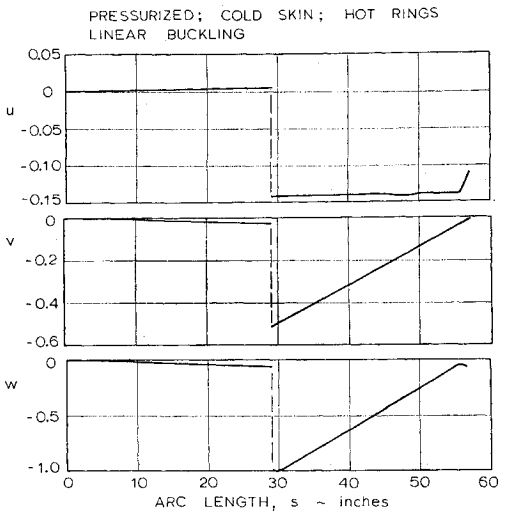

Fig. 11 Buckling mode for $n = 2$ circumferential waves corresponding to shell which is torn between Segments 2 and 3; $p_{cr} = 18.4$ psi.

as to reduce its meridional curvature, thereby making it resemble more closely the "simplified" model of the view A-A in Fig. 8. It is seen that the calculated buckling pressures for the $n = 2$ buckling mode are very sensitive to temperature distribution and geometry of the end A-A of the shell.

It appears that the experimental buckling pressure of 35 psi cannot be predicted unless one assumed that the structure was damaged during the prebuckling deformations. That some plastic flow occurred near the beginning of Segment 3 is clear from the high meridional stresses there shown in Fig. 9. If one assumes that the shell tears at this point, so that the buckling displacements u, v, and w and rotation χ need no longer be continuous, one obtains a buckling load of 18.4 psi with two circumferential waves. Figure 11 shows the mode shape.

References

[1] Hoff, N. J., "Buckling at High Temperature," *Journal of the Royal Aeronautical Society*, Vol. 61, 1957, pp. 756–774.

[2] Abir, D. and Nardo, S. Y., "Thermal Buckling of Circular Cylindrical Shells Under Circumferential Temperature Gradients," *Journal of the Aeronautical Sciences*, Vol. 26, 1959, pp. 803–808.

[3] Ross, B., Hoff, N. J., and Horton, W. H., "The Buckling Behavior of Uniformly Heated Thin Circular Cylindrical Shells," *Experimental Mechanics*, Vol. 6, 1966, pp. 529–537.

[4] Lu, S. Y. and Chang, L. K., "Thermal Buckling of Conical Shells," *AIAA Journal*, Vol. 5, No. 10, Oct. 1967, pp. 1877–1882.

[5] Chang, L. K. and Lu, S. Y., "Nonlinear Thermal Elastic Buckling of Conical Shells," *Nuclear Engineering and Design*, Vol. 7, 1968, North-Holland Publishing Co., Amsterdam, pp. 159–169.

[6] Hoff, N. J., "Buckling of the Thin Cylindrical Shell Under Hoop Stresses Varying in Axial Direction," *Journal of Applied Mechanics*, Vol. 24, 1957, pp. 405–412.

[7] Anderson, M. S., "Thermal Buckling of Cylinders," *Collected Papers on Instability of Shell Structures*, TN D-1510, NASA, Dec. 1962, pp. 266–276.

[8] Johns, D. J., "Local Circumferential Buckling of Thin Circular Cylindrical Shells," *Collected Papers on Instability of Shell Structures*, TN D-1510, NASA, Dec. 1962, pp. 266–276.

[9] Cohen, G. A., "Computer Analysis of Asymmetric Buckling of Ring-Stiffened Orthotropic Shells of Revolution," *AIAA Journal*, Vol. 6, No. 1, Jan. 1968, pp. 141–149.

[10] Kalnins, A., "Analysis of Shells of Revolution Subjected to Symmetrical and Nonsymmetrical Loads," *Journal of Applied Mechanics*, Vol. 31, 1964, pp. 467–476.

[11] Witmer, E. A. et al., "An Improved Discrete-Element Analysis and Program for the Linear-Elastic Static Analysis of Meridionally-Curved, Variable-Thickness Branched Thin Shells of Revolution Subjected to General External Mechanical and Thermal Loads," Part 1: "Analysis and Evaluation," SAMSO TR 68-310; also ASRL TR-146-4, March 1968, Aeroelastic and Structures Research Lab., Dept. of Aeronautics and Astronautics, M. I. T., Cambridge, Mass.

[12] Stern, P., "Stresses and Displacements in Elastic-Plastic Shells of Revolution with Temperature-Dependent Properties," Rept. 6-90-62-123, Jan. 1963, Lockheed Missiles & Space Co.,

[13] Bushnell, D., "Stress, Stability, and Vibration of Complex Shells of Revolution: Analysis and User's Manual for BOSOR3," Rept. N-5J-69-1, Sept. 1969, Lockheed Missiles & Space Co.

[14] Stein, M., "The Effect on the Buckling of Perfect Cylinders of Prebuckling Deformations and Stresses Induced by Edge Support," *Collected Papers on Instability of Shell Structure*, TN D-1510, NASA, Dec. 1962, p. 217.

[15] Budiansky, B. and Anderson, D. G. M., "Numerical Shell Analysis—Nodes Without Elements," 12th International Congress of Applied Mechanics, Stanford Univ., Palo Alto, Calif., August 26–31, 1968.

[16] Brogan, F. A. and Almroth, B. O., "Buckling of Cylinders With Cutouts," *AIAA Journal*, Vol. 8, No. 2, Feb. 1970, pp. 236–240.

[17] Johnson, D. E., "A Difference-Based Variational Method for Shells," *International Journal of Solids and Structures*, Vol. 6, 1970, pp. 699–724.

[18] Bushnell, D., "Analysis of Ring-Stiffened Shells of Revolution Under Combined Thermal and Mechanical Loading," *Proceedings of AIAA/ASME 11th Structures, Structural Dynamics, and Materials Conference*, AIAA, New York, 1970, pp. 195–210.

[19] Bushnell, D., "Analysis of Buckling and Vibration of Ring-Stiffened, Segmented Shells of Revolution," *International Journal of Solids and Structures*, Vol. 6, 1970, pp. 157–181.

[20] Fulton, R., personal communication, Oct. 1969, NASA-Langley, Hampton, Va., who used an independently developed computer code, BALORS-SALORS, to calculate buckling loads of heated cylinder.

[21] Cohen, G., personal communication, Jan. 1970, Structures Research Associates, Newport Beach, Calif., who used the computer code described in Ref. 9 to calculate buckling loads of heated cylinder.

[22] Jones R. M., and McKinley, T., personal communication, July, 1969, Aerospace Corp., San Bernardino, Calif.